

Elastic Properties of External Cortical Bone in the Craniofacial Skeleton of the Rhesus Monkey

Qian Wang and Paul C. Dechow*

Department of Biomedical Sciences, Baylor College of Dentistry, Texas A&M University Health Sciences Center, Dallas, Texas 75246

KEY WORDS bone; biomechanics; function; adaptation

ABSTRACT Knowledge of elastic properties and of their variation in the cortical bone of the craniofacial skeleton is indispensable for creating accurate finite-element models to explore the biomechanics and adaptation of the skull in primates. In this study, we measured elastic properties of the external cortex of the rhesus monkey craniofacial skeleton, using an ultrasonic technique. Twenty-eight cylindrical cortical specimens were removed from each of six craniofacial skeletons of adult *Macaca mulatta*. Thickness, density, and a set of longitudinal and transverse ultrasonic velocities were measured on each specimen to allow calculation of the elastic properties in three dimensions, according to equations derived from Newton's second law and Hooke's law. The axes of maximum stiffness were determined by fitting longitudinal velocities measured along the perimeter of each cortical specimen to a sinusoidal function. Results showed

significant differences in elastic properties between different functional areas of the rhesus cranium, and that many sites have a consistent orientation of maximum stiffness among specimens. Overall, the cortical bones of the rhesus monkey skull can be modeled as orthotropic in many regions, and as transversely isotropic in some regions, e.g., the supraorbital region. There are differences from human crania, suggesting that structural differences in skeletal form relate to differences in cortical material properties across species. These differences also suggest that we require more comparative data on elastic properties in primate craniofacial skeletons to explore effectively the functional significance of these differences, especially when these differences are elucidated through modeling approaches, such as finite-element modeling. *Am J Phys Anthropol* 000:000–000, 2006.

© 2006 Wiley-Liss, Inc.

Craniofacial skeletons are designed to perform many functions. In addition to housing the brain itself, the skull houses special sense organs for vision, smell, hearing, and taste, and it reflects their functional demands in shape and structure (Shipman et al., 1985). How function and morphology relate to each other can be probed through the investigation of the behavior of craniofacial bones under physiological loading conditions, such as during mastication, by *in vivo* bone strain experiments (Hylander and Johnson, 1997; Ross, 2001; Wang et al., 2005). Finite-element analysis (FEA) is a powerful tool in probing the interface between function and morphology, as it is able to estimate synchronous strain across an entire structure, and enable interpretation of strain data from a global perspective. The accuracy and validity of FEA of the craniofacial skeleton can be improved with specific knowledge of cranial-bone material properties and their variation (Strait et al., 2005).

Elastic structure in remodeled cortical bone was suggested to exhibit orthotropic elastic symmetry, which means that in three mutually perpendicular planes defined by three axes, the elastic moduli are uniform in one direction, but different along each axis (Reilly and Burstein, 1975; van Buskirk et al., 1981; Ashman, 1982; Ashman et al., 1984). This is likely true in many cortical regions. However, within this structural framework, elastic properties may vary within and between bones of individuals. For example, bone material properties vary throughout a skull, or a mandible (Yamada and Evens, 1970; Papadimitriou et al., 1996; Peterson and Dechow, 2003; Schwartz-Dabney and Dechow, 2003; Wang and Dechow, 2004). Different species with different bone shapes and structures might have different material

properties, suggesting that structural differences in skeletal form relate to differences in cortical material properties across species. For example, there are different patterns of variation in elastic properties throughout a human mandible compared to a baboon mandible (Wang and Dechow, 2004). In the human skull, Peterson and Dechow (2003) found few differences in elastic properties among different bones of the human cranium. However, their results show that most muscle-bearing sites are stiffer along the axis of maximum stiffness than are non-muscle-bearing sites, and that cortical bones in close vicinity (though in different cranial bones) often have similar material properties, such as in sites along the coronal sutures in the frontal and parietal bones (Peterson and Dechow, 2003). These results suggest an adaptive or developmental relationship between the elastic structure and function of cortical bone in specific skeletal regions (Peterson and Dechow, 2003; Wang and Dechow, 2004).

The characteristics and variation of the three-dimensional material properties of cortical bone in primate

Grant sponsor: NSF; Grant number: BCS 0240865.

*Correspondence to: Dr. Paul C. Dechow, Department of Biomedical Sciences, Baylor College of Dentistry, 3302 Gaston Ave., Dallas, TX 75246. E-mail: pdechow@bcd.tamhsc.edu

Received 22 August 2005; accepted 24 January 2006.

DOI 10.1002/ajpa.20438
Published online in Wiley InterScience
(www.interscience.wiley.com).

skulls are largely unexplored, except for recent systematic work on human dentate and edentulous skulls (Schwartz-Dabney and Dechow, 2002a, 2003; Peterson, 2002; Peterson and Dechow, 2002, 2003), and some work on nonhuman primates, such as baboons and rhesus monkeys (Dechow and Hylander, 2000; Wang and Dechow, 2004). The principal purposes of this study are to evaluate the thickness, density, material properties, and their variations in the cortical bone of the rhesus monkey craniofacial skeletons. The rhesus monkey (*Macaca mulatta*) has been widely used for medical, biological, biomechanical, and anthropological research (e.g., Bourne, 1975; DeRousseau, 1988; Schneiderman, 1992), and has often been used as a model for studies of primate craniofacial function, such as investigations of occlusal force (Dechow and Carlson, 1990), in vivo and in vitro studies of bone strains during chewing and biting (Behrents et al., 1978; Hylander and Johnson, 1997), and investigation of the preferential orientations of collagen in the circumorbital area (Bromage and Boyde, 1998).

The orientation of maximum stiffness in cortical bone and the anatomical axis of the skeletal structure are assumed to be coincident in long bones. This is not the case in human cranial bone (Peterson and Dechow, 2003), and is also likely not true in crania of other mammals. In macaque mandibles and human femora, Haversian canals and most collagen fibrils are oriented parallel to the long axis (Bromage, 1992, 1993; Bromage et al., 2003; Goldman et al., 2003). These findings lead to the presumption that the orientation of maximum stiffness of cortical bone runs parallel to the anatomical axis of the bone. However, in macaque mandibles, the axis of maximum stiffness is always found to be at some angle to the long axis of the bone, which may decrease deformation during torsion (Dechow and Hylander, 2000). The facial skeleton undergoes certain degrees of torsion during mastication (Ross and Metzger, 2004); it might also bear this deviation.

In a previous study (Dechow and Hylander, 2000), we reported on the elastic properties of cortical bone from the macaque mandibular corpus inferior to the molar region, to assess the impact of elastic property variation on stress-strain relationships during function. Little else is known about elastic property variation in the cranial skeletons of rhesus monkeys or other nonhuman primates.

Our first objective was to determine elastic properties in different anatomical regions throughout the rhesus monkey cranium. Then we assessed this variation in cortical elastic properties, with a view to evaluating its functional implications. We divided the rhesus monkey cranium into several functional areas, based on the structure of the monkey skull. Our final objective was to compare elastic properties between different species. Preliminary studies in our laboratory inferred similarities in elastic properties of mandibular cortical bone between more distantly related taxa, such as humans, baboons, and pigs (i.e., Dechow and Hylander, 2000; Wang and Dechow, 2004). Here, we compare cortical elastic properties in rhesus monkey skulls to existing data from human crania previously collected in our laboratory (Peterson, 2002; Peterson and Dechow, 2003). The human data set is the only comparable data set from vertebrate crania.

MATERIALS AND METHODS

The sample consisted of six rhesus monkey crania, of which two were from adult males; the rest were from

adult females (Table 1). All animal tissues were obtained from the Regional Primate Research Center (RPRC) at the University of Washington (supported by NIH grant RR00166). Animal tissue use conformed to all NIH, state, and federal standards. All crania lacked evidence of bone disease, and all permanent maxillary teeth were in situ in all crania. The crania were stored in freezers at -20°C prior to removal of bone specimens. This process has an insignificant impact on ultrasonic measurements of elastic properties (Evans, 1973; Zioupos et al., 2000).

There are several ways of organization of the craniofacial skeleton, depending on research interests in growth, function, or both (e.g., Moss, 1976). Since we intended to examine the variation of material properties in different functional areas, we divided the rhesus monkey cranium into seven anatomical areas, based on their obvious or alleged functions. These were:

1. Vault (Val): the calvarial portion of the frontal bone, parietal bone, and greater wing of the sphenoid bone. The principal functions of this area are protecting the brain, and providing anchorage for the temporalis muscle (Sullivan, 1961).
2. Circumorbital area (Orb): skeletal structures encircling the external portion of the eye, including the supraorbital torus of the frontal bone, and the frontal process of the zygomatic bone. The principal functions of this area are to protect the eyes and transmit forces produced by mastication and biting (Endo, 1966, 1970; Rak, 1983; but see Ravosa, 1991a,b; Ravosa et al., 2000).
3. Zygomatic arch (Zyg): the beam connecting the lateral part of face and the skull. Its principal function is to provide attachment for the masseter muscles (Hylander and Johnson, 1997).
4. Muzzle (Muz): the superior lateral part of the snout, including the nasal bone, premaxilla, and maxilla. This part protects the nasal cavity, and transmits stresses induced by bite force (Rak, 1983).
5. Intraorbital area (Ino): four internal walls of the orbit, jointly formed in large part by frontal, maxillary, and sphenoid bones. This area protects the eyes (Ross, 2001).
6. Alveolus (Alv): the inferior lateral part of the snout, formed by the maxilla and premaxilla. This area represents the hosting organ for the maxillary dentition.
7. Palatine process of the maxilla (Pal): the anterior portion of the hard palate in the oral cavity, formed by the palatine processes of the maxillary bones.

Twenty-eight cylindrical cortical bone samples were harvested from the cortical bone of the outer surface of the right half of each cranium (Fig. 1). Sites 1–6, 9–10, and 12 were collected from the vault (Val); sites 11 and 13–14 were collected from the zygomatic arch (Zyg); sites 7–8 and 15 were from the circumorbital region (Orb); sites 16–18 were from the muzzle area (Muz); sites 19–22 were from the alveolar process of the maxilla (Alv); sites 23–26 were from the inner wall of the orbit (Ino); and sites 27–28 were from the roof of the oral cavity, i.e., the palatine process of the maxilla (Pal). In the vault, sites 1–4 were collected from the parietal bone; sites 5–6 were from the calvarial portion of the frontal bone; sites 9–10 were from the squamous portion of the temporal bone; and site 12 was from the greater wing of the sphenoid bone.

TABLE 1. Craniometric measurements¹

Cranium	1 (female)	2 (female)	3 (female)	4 (female)	5 (male)	6 (male)
g-op	88.6	90.2	85.6	86.5	101.3	99.9
eu-eu	67.8	71.9	57.7	61.5	73.4	79.2
ba-b	55.4	59.9	52.0	54.4	64.7	63.2
enba-n	65.6	64.6	66.2	64.6	77.5	76.7
enba-pr	73.2	82.5	82.3	76.6	109.5	109.9
fmt-fmt	66.2	71.8	63.5	67.5	84.7	90.2
n-pr	39.9	46.6	43.5	40.7	52.5	55.0
zm-zm	54.4	56.8	53.9	55.3	68.9	66.6
zy-zy	76.8	85.7	77.6	78.3	112.0	100.7
pr-alv	41.9	46.7	45.1	44.9	63.2	57.6
ecm-ecm	38.0	38.7	39.1	39.4	47.0	46.1
ol-sta	38.2	49.6	43.6	38.9	65.3	57.7
enm-enm	20.2	24.8	22.3	24.7	30.6	27.9
Palatal height	5.1	7.0	6.7	7.1	9.7	10.7

¹ Unit: mm. alv, alveolon; b, bregma; ba, basion; ecm, ectomalare; enbar, endobaion; enm, endomalre; eu, euryon; fmt, frontomalar temporale; g, glabella; n, nasion; ol, orale; op, opisthokranion; pr, prosthion; sta, staphylion; zm, zygomaxillare; zy, zygon.

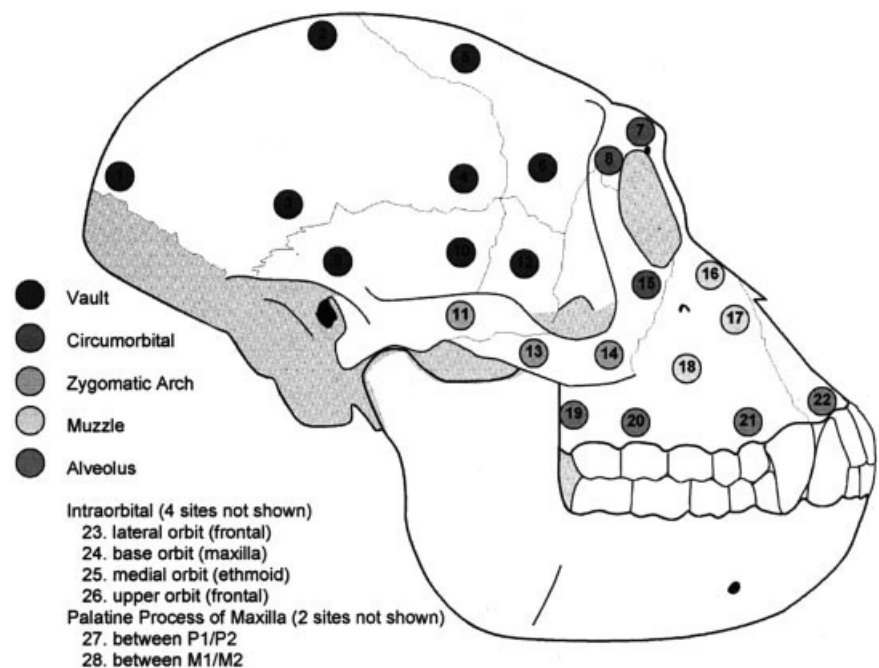


Fig. 1. Location of cortical specimen in lateral view. Each site is numbered for reference (site numbers identified in text).

Sites were marked with a graphite line to indicate orientation of the bone specimens. As described in a previous study of cortical bone from the human cranium (Peterson and Dechow, 2003), the standard orientation of the graphite line varied, depending on the region of the skull from which the specimen was removed. In the cranial vault, the line on each bone specimen paralleled the sagittal suture (sites 1–10 and 12); in the zygomatic arch, the line parallel to the long axis of the arch (site 11 and 13–14); and in the face, the line was perpendicular to the functional occlusal plane (FOP), defined by biting points of the second molar (M^2) and third premolar (P^3) (Thayers, 1990) (sites 15, and 18–21), or to the margin of the alveolar process (sites 16–17 and 22). In the inner orbital area, the line was perpendicular to the orbit rim (sites 23–26). In the palate, the line paralleled the midpalatal suture (sites 27–28). The line was oriented with an arrowhead, indicating a superior or anterior direction. Bone cylinders with a diameter of 4 mm were harvested by means of a slow-speed dental hand-

piece and trephine burs. We previously showed that the resulting cylindrical-shaped specimens improve the accuracy of elastic property measurement (Schwartz-Dabney and Dechow, 2002b) because they allow a determination of the orientation of the orthotropic axes of the specimen. In a minority of specimens, it was necessary to remove endosteal cancellous bone by grinding until there was no visible porosity on the endosteal surface. Specimens were kept cool with a water drip during this procedure. Samples were stored in equal proportions of 95% ethanol and isotonic saline, as this storage medium has little effect over time on measured ultrasonic velocities and the elastic coefficients derived from these measurements (Ashman et al., 1984; Zioupos et al., 2000; Schwartz-Dabney and Dechow, 2002a, 2003).

All bone cylinders were measured with digital calipers to the nearest 0.01 mm to verify diameter (4 mm) and determine cortical thickness, which is defined as the distance from the external cortical surface to the internal cortical-trabecular interface (Schwartz-Dabney and De-

chow, 2003). Apparent density calculations in mg/cm^3 , based on Archimedes' principal of buoyancy, were calculated based on bone weight measurements taken to the nearest 0.001 g with a Mettler-PM460 analytical balance and densitometry kit (Mettler, Toledo, OH).

Our ultrasonic measurement technique was described in detail by Schwartz-Dabney and Dechow (2003). Ultrasonic waves were generated with a Hewlett-Packard pulse generator and mounted piezoelectric transducers (2.25 MHz longitudinal, Panametrics V-156-RM and 5.0 MHz transverse, Panametrics-NDT, Waltham, MA). Time delays were measured with an oscilloscope (Tektronix TDS 420, Garland, TX) by phase comparison of the signal before and after its transmission through a specimen. Ultrasonic velocities were calculated by dividing the specimen thickness or diameter by the recorded time delay minus the constant system delay.

Our method of determining the axes of minimum and maximum stiffness in the plane of the cortical plate was refined from our previously described methods (Peterson and Dechow, 2002; Schwartz-Dabney and Dechow, 2002a, 2003). As in our previous work, the direction of the axis of maximum stiffness in the plane of the cortical plate corresponded with the direction of peak longitudinal velocity in that plane. Likewise, the direction of the axis of minimum stiffness in the plane of the cortical plate corresponded to the lowest velocity in that plane. In an orthotropic elastic solid, these two axes are perpendicular to each other. The method that we used previously entailed using the maximum and minimum velocities among nine velocities measured at angular intervals of 22.5° around the circumference of the cylindrical specimen. We then confirmed the validity of the values by checking to see that they matched the proper pattern, i.e., that the maximum and minimum velocities were always orthogonal to each other. As the rotation interval is 22.5° , the real axis of maximum stiffness is the selected axis with an angular error up to $\pm 11.25^\circ$. A theoretical analysis of "off-axis" velocity measurement through cubic specimens predicted errors of 1.3% in elastic moduli and 5.0% in shear moduli for measurements taken at 10° "off-axis," and this error exponentially increased to 4% and 18%, respectively at 20° "off-axis" (Turner and Cowin, 1988). To minimize the angular errors incurred by this direct method and to base our longitudinal velocities on all measured velocities, we used a program written in Mathcad to fit the data for each bone specimen to a sine function [$a * \sin(X + b) + c$]. The coefficients a, b, and c corresponded to the orientation of the axes of maximum stiffness, the average velocity, and the maximum deviation of the curve from the average velocity. The direction of the axis of maximum stiffness corresponded with the direction of peak longitudinal velocity (D_3). Likewise, the minimal principal axis, or least stiffness direction, corresponded to the lowest velocity (D_2). The third axis (D_1) was always tangential or perpendicular to the cortical plane. These three axes defined the orthotropic elastic planes of the cortical bones, and measurements of transverse velocities were conducted on planes formed by them.

Elastic properties were calculated from elastic coefficients. The latter were derived from cortical density, and longitudinal and transverse velocities were based on mathematical relationships derived from the principles of linear elastic wave theory and Hooke's law, according to previously described methods (van Buskirk et al., 1981; Ashman, 1982; Ashman et al., 1984). Relationships

and definitions for elastic coefficients and the derived material properties are described in detail elsewhere (Ashman et al., 1984; Dechow et al., 1993). Briefly, the elastic modulus (E) measures axial stiffness or the amount of deformation (strain) relative to an applied load (stress). Subscripts, i.e., E_1 , E_2 , or E_3 , indicate the appropriate axis for each elastic modulus. E_1 , E_2 , and E_3 are elastic moduli along different axis. Similarly, subscripts indicate the orientation for shear moduli and Poisson ratios. Shear modulus (G) measures stiffness in shear or angular deformation relative to applied shearing loads in a plane between two axes indicated by subscripts (G_{12} , G_{31} , or G_{32}). Poisson's ratio (ν) is a measure of stiffness of a structure perpendicular to that of the applied load. It is a ratio of the strain in the secondary direction (response direction) divided by strain in the primary direction (applied load direction). The first subscript indicates the axis of the applied load, and the second subscript indicates the response direction, i.e., ν_{12} , ν_{13} , ν_{21} , ν_{23} , ν_{31} , and ν_{32} . In our study, elastic properties were calculated from original data such as density and ultrasonic velocities, using a program written in Mathcad. Ultrasonic velocities and densities were used to calculate 6×6 matrices, or "c" matrices, including nine unique elastic coefficients (c_{11} , c_{22} , c_{33} , c_{44} , c_{55} , c_{66} , c_{12} , c_{13} , and c_{23}) and then 12 technical constants (three elastic moduli: E_1 , E_2 , and E_3 ; three shear moduli: G_{12} , G_{31} , G_{23} ; and six Poisson ratios: ν_{12} , ν_{21} , ν_{13} , ν_{31} , ν_{23} , and ν_{32}). A consequence of the assumption of orthotropic material symmetry is that $\nu_{ji}E_i = \nu_{ij}E_j$. Thus, Poisson's ratios can be simplified and presented as three rather than six values. These are given here as ν_{12} , ν_{13} , and ν_{23} . We also compared relative stiffness between axes by using ratios of elastic constants, such as E_1/E_2 , E_1/E_3 , and E_2/E_3 , to quantify anisotropy in three cortical planes.

The error of the method was assessed in several ways. For individual specimens, the measurement error of ultrasonic velocities was evaluated by repeated measurements of the same specimen in an identical orientation. The measurement error was 2.1% for longitudinal velocities, and 3.1% for transverse velocities, indicating a high reliability of measurements. Errors in the three major longitudinal velocities (V_{11} , V_{22} , and V_{33}) along orthogonal directions primarily affect the final results of corresponding elastic moduli, i.e., V_{11} affects E_1 , V_{22} affects E_2 , and V_{33} affects E_3 . For example, if the velocity in the direction of maximum stiffness (V_{33}) is 2.1% lower than the real value, while other variables remain the same, then there is almost no change in E_1 (0.04% lower) and E_2 (0.37% lower), while E_3 is most altered (3.3% lower). Errors in transverse velocity have a different effect on calculated elastic properties. For example, if transverse velocities V_{23} and V_{32} are 3.1% lower than the real values (V_{23} and V_{32} should not be confused with ν_{23} and ν_{23} ; V represents velocity here, while ν represents Poisson's ratio), there is no effect on technical constants G_{12} and G_{31} . E_1 changes slightly (1.19% higher), small and equal changes are found for E_2 and E_3 (2.93% lower), and G_{23} changes the most (5.9% higher). However, none of these changes are statistically significant. For individual sites, measurement error was assessed by calculating the percent ratio between the variance of the method error (squared Dahlberg's error) and the population variance of that measurement (squared standard deviation) (Cooke and Wei, 1991). For longitudinal velocities, the error percentage was always less than 8.3% of

TABLE 2. Cortical density and thickness

Area	Site	N	Density (mg/cm ³)		Thickness (mm)		
			Mean	SD	Mean	SD	
Val	1	6	1,631.3	158.4	2.44	0.38	
	2	6	1,709.5	139.0	2.21	0.43	
	3	6	1,854.5	153.7	2.21	0.41	
	4	5	1,789.4	139.4	1.77	0.37	
	5	6	1,600.5	218.8	2.47	0.63	
	6	6	1,706.3	118.0	2.22	0.43	
	9	6	1,722.5	134.3	1.85	0.57	
	10	6	1,672.7	205.5	1.89	0.64	
	12	6	1,620.7	141.9	1.47	0.22	
	Total		53	1,699.2	166.7	2.06	0.54
	Orb	7	6	1,527.8	153.6	2.90	0.50
		8	6	1,498.3	116.5	2.72	0.58
15		6	1,678.5	166.6	2.34	0.69	
Total		18	1,568.2	160.3	2.65	0.61	
Zyg	11	5	1,531.5	177.7	2.11	0.46	
	13	6	1,719.3	280.4	1.71	0.60	
	14	6	1,689.5	164.7	1.73	0.44	
	Total		17	1,640.9	223.4	1.84	0.51
Muz	16	6	1,581.5	137.9	2.46	0.53	
	17	6	1,611.2	132.8	2.20	0.64	
	18	6	1,697.2	203.8	1.00	0.33	
	Total		18	1,629.9	159.8	1.88	0.81
Alv	19	6	1,771.7	328.9	1.11	0.60	
	20	6	1,762.2	61.1	2.12	0.77	
	21	6	1,517.2	110.0	2.03	0.40	
	22	6	1,687.3	259.5	1.73	0.59	
	Total		24	1,684.6	229.1	1.75	0.70
Ino	23	4	1,825.3	324.9	0.69	0.08	
	24	6	1,584.8	199.1	2.30	0.84	
	25	5	1,635.4	372.1	1.30	0.62	
	26	6	1,785.2	158.7	2.29	0.38	
	Total		21	1,699.9	264.7	1.75	0.86
Pal	27	6	1,785.2	118.8	1.18	0.16	
	28	6	1,739.1	151.3	1.01	0.07	
Total		12	1,762.2	131.9	1.09	0.15	
ANOVA			F	P	F	P	
Area			1.75	NS	9.39	0.01	
Site			1.56	0.05	6.57	0.01	

the total biological variance; for transverse velocities, the error percentage was always less than 13.3% of the total biological variance.

Data were analyzed using Minitab statistical analysis program 14.1 (Minitab, Inc., State College, PA) and the SYSTAT statistical analysis program (release 10, SPSS, Inc., Chicago, IL). Descriptive statistics, including means, standard deviations (SDs), and standard errors of means (SEMs), were calculated for all measurements. Correlation coefficients were also calculated to examine relationships between selected variables. A series of one-way analysis of variance (ANOVA) tests was performed to assess differences among areas and sites. No post hoc tests were reported, due to the large numbers of results incurred by paired comparisons among the seven areas and 28 sites. Angular measurements (orientation of maximum stiffness) were analyzed with circular descriptive statistics, including the mean angles, circular SD, and Rayleigh's test of uniformity (Zar, 1999), with the Oriana Statistical Analysis Program (version 2.02, Kovach Computing Services, Anglesey, Wales, UK). Rayleigh's test of uniformity revealed whether a site actually had a significant mean angle (oriented site), or whether the distribu-

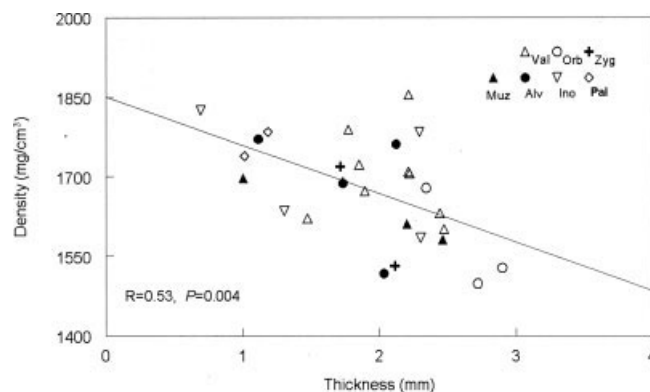


Fig. 2. Scatterplot of mean thickness vs. density by site. Linear regression: Density = $-91.440 * \text{Thickness} + 1,850.854$, $r = 0.53$, $P = 0.004$.

tion of angles between individuals could not be distinguished from a random distribution (nonoriented site). Significance levels were set at $\alpha = 0.05$, except in calculations of the dominant orientations of maximum stiffness, where several average angular values were reported, though the P -value might be higher than 0.05, as discussed below.

RESULTS

Density varied significantly among sites ($P = 0.01$), but not among areas (Table 2). The average density by site ranged from 1,498 mg/cm³ (site 8 in the orbital region: frontal bone) to 1,854 mg/cm³ (site 3 in the vault: parietal bone), but most were between 1,500–1,700 mg/cm³.

Significant differences were also found for thickness of the external cortical plate among sites and areas ($P \leq 0.05$), but the differences within areas were smaller than among areas (Table 2). The external cortex was thickest in the circumorbital area, with a grand mean of 2.65 mm across three sites. Site 7, located at the middle part of the supraorbital torus on the frontal bone (2.90 mm), had the thickest cortical bone of any site. On average, cortical bone was thinnest on the palatine process of the maxilla (sites 27–28), averaging 1.09 mm (this area was significantly thinner than other regions). Site 23 in the inner orbital region had the thinnest cortical bone of any site (0.69 mm). There was similar variation throughout the crania in external cortical thickness in both male and female animals, and there were no significant differences between males and females.

Thickness and density are both major factors in the structural mechanics of cortical bone, and they showed a significant but low negative correlation in our sample ($r = 0.25$, $P = 0.004$), but this was higher for mean values ($r = 0.53$, $P = 0.004$) (Fig. 2). Overall, bone from most regions had similar variation, except for that from the circumorbital region (mostly thicker and less dense) and palatine region (thinner and denser).

The values for elastic moduli demonstrated differences by direction, in that E_3 was larger than E_2 , which was larger than E_1 (Table 3, Figs. 3–5). When elastic moduli were analyzed separately (Fig. 4), both E_1 and E_2 showed significant differences among areas ($P < 0.05$), but not among sites within areas (Table 4), while E_3 showed no significant difference among either areas or sites.

TABLE 3. Elastic moduli

Area	Site	N	E ₁ (GPa)		E ₂ (GPa)		E ₃ (GPa)		
			Mean	SD	Mean	SD	Mean	SD	
Val	1	6	9.4	3.9	12.0	3.7	14.4	4.2	
	2	5	10.0	3.9	12.3	3.9	16.5	5.2	
	3	5	13.7	8.0	16.4	6.6	20.0	8.6	
	4	4	10.6	4.3	13.9	4.2	16.5	5.9	
	5	5	7.9	3.8	11.0	5.0	14.9	7.8	
	6	6	10.6	4.1	13.3	3.9	16.3	5.6	
	9	5	11.5	3.1	16.2	5.1	20.3	6.8	
	10	6	9.4	4.8	12.9	5.0	18.5	6.3	
	12	5	7.8	5.3	10.0	5.4	13.0	6.1	
	Total		47	10.1	4.6	13.1	4.8	16.7	6.2
	Orb	7	6	9.1	2.3	9.7	2.1	14.4	2.9
		8	6	10.2	2.9	11.2	3.1	13.1	4.2
15		4	11.3	3.6	13.1	3.3	19.8	8.2	
Total		16	10.1	2.8	11.1	2.9	15.2	5.5	
Zyg	11	3	8.2	2.7	10.0	2.9	12.5	0.9	
	13	4	8.6	4.7	12.4	5.7	20.8	8.3	
	14	4	8.9	2.9	10.9	4.4	17.9	3.0	
	Total		11	8.6	3.3	11.2	4.3	17.5	5.9
Muz	16	2	13.5	0.5	14.7	0.7	22.6	0.8	
	17	4	10.9	3.7	13.2	3.5	17.1	5.4	
	18	4	11.5	5.3	14.4	5.4	18.1	5.4	
	Total		10	11.7	3.9	14.0	3.8	18.6	4.9
Alv	19	3	12.8	5.2	15.7	4.3	19.8	4.7	
	20	6	12.4	2.6	15.1	3.7	21.3	4.1	
	21	6	9.9	3.9	12.1	4.0	16.7	3.0	
	22	4	10.0	1.4	13.9	3.9	18.5	1.7	
	Total		19	11.2	3.4	14.0	3.8	19.0	3.7
Ino	23	4	9.4	3.8	14.5	3.4	17.6	4.9	
	24	6	8.6	2.8	10.5	2.3	15.7	4.3	
	25	3	7.1	4.4	11.5	6.5	14.6	8.9	
	Total		17	9.4	3.9	13.1	5.1	16.5	5.6
Pal	27	6	7.5	1.4	8.8	1.5	15.3	4.2	
	28	6	6.4	1.0	7.5	1.5	18.8	7.9	
	Total		12	7.0	1.3	8.2	1.6	17.0	6.3
ANOVA			F	P	F	P	F	P	
Area			2.18	0.049	3.41	0.004	0.86	NS	
Site			1.04	NS	1.53	NS	0.96	NS	

The palatine process had the lowest mean E₁ (7.0 GPa; unit: 1 GPa = 10⁹ N/m²). The muzzle area and the alveolar area had the largest mean E₁ (>11.0 GPa). Site 3 in the vault (parietal bone) had a higher E₁ (13.7 GPa) than any other site, followed by site 16 in the muzzle area (13.5 GPa). Similar patterns of variation were observed for E₂, with minimum stiffness on the cortical plane. The palatine process had the lowest minimum stiffness (8.2 GPa), while the highest values were observed in the muzzle and alveolar areas (14.0 GPa).

Significant differences among sites were also found for the anisotropy represented by three ratios: E₁/E₂, E₁/E₃, and E₂/E₃. Significant differences were found among areas for E₁/E₂ and E₂/E₃ (Table 4, Fig. 5). For E₁/E₂, the circumorbital area had weak anisotropy (0.91), the rest of the areas had moderate anisotropy, and most anisotropic was the inner orbital area (0.72). A scatterplot of mean values of E₂ vs. E₃ (Fig. 5) demonstrated a correlation ($r = 0.62$, $P < 0.001$). Within the range of the plot, the largest anisotropy (E₂/E₃) was found in the palatine process of the maxilla (0.52) and the zygomatic arch (0.64). The least anisotropy (E₂/E₃) was found in the vault (0.79) and inner orbital area (0.80) (Table 4, Fig. 5).

The patterns of variation in the magnitude of bone stiffness in three orthogonal directions can be visualized by a triangle plot of the percentage of E₁, E₂, and E₃ when their sums are scaled to 1.0 (Fig. 6). Figure 6 demonstrates the difference of cortical elastic moduli along three principal axes, and how this difference varies regionally. The inner orbital, vault, alveolar, and muzzle areas have similar patterns of variation (0.25/0.33/0.42), while the remaining three areas have different patterns. The palatine process of the maxilla has relatively small E₁ and E₂ compared to E₃; the zygomatic arch has a similar pattern, but to a lesser degree. The differences between E₁ and E₂ are relatively small in the circumorbital area.

No correlation was observed among cortical thickness, elastic moduli, and anisotropy, except for a moderate correlation ($r = 0.55$, $P = 0.003$) indicating that E₁/E₃ anisotropy decreased as cortical thickness increased (Fig. 7).

Axes of maximum stiffness varied significantly among sites and areas ($P < 0.01$) (Table 5, Figs. 3, 8). Rayleigh's test for uniformity demonstrated significant mean directions of maximum stiffness at 12 sites. Because of the variability of the angular dispersion, the other 16 sites did not show any significant mean direction. However, 12 sites had a dominant axis, which means that an identical or similar orientation was observed in at least three crania among six individuals (Table 5, Fig. 8). In general, the orientation of maximum stiffness in the alveolar, muzzle, and vault areas ran superoinferiorly, and along the orientation of the zygomatic arch and the supraorbital torus. For example, on the supraorbital torus, the axis of site 7 was oriented 11.4° to the coronal plane; the axis of site 8 was oriented 14.1° to the coronal plane.

Generally, cortical bones at sites with higher anisotropy tend to have a consistent orientation of maximum stiffness in the plane of the cortical plate. On average, sites with a significant mean axis of E₃ have lower ratios of E₂/E₃ (mean 0.709 ± SE 0.019, N = 57) than those sites without a constant orientation of E₃ (mean 0.761 ± SE 0.015, N = 76) ($P = 0.04$).

There were significant differences for G₁₂, G₃₁, and G₂₃ among areas, but not among sites within areas (Table 6, Fig. 9). The source of area differences principally came from the palatine area, which had relatively low values. On average, means of G₃₁ (2.6–5.6 GPa) were larger than those of G₁₂ (2.8–8.4 GPa), and smaller than those of G₂₃ (3.6–10.9 GPa). Overall, the smallest shear moduli values were found in the palatine process of the maxilla, and the largest values were in the muzzle and alveolar areas.

The Poisson ratios showed no significant differences among either areas or sites (Table 7, Fig. 10). In terms of magnitude, ν_{12} is bigger than ν_{13} , and the latter is bigger than ν_{23} .

DISCUSSION

Regional variation and functional implications

Our results demonstrated patterns of variation in material properties of cortical bone in the macaque craniofacial skeleton. Cortical thickness, E₁, E₂, all shear moduli, and anisotropy vary among areas. The vault, muzzle, and inner orbital areas are less anisotropic than other areas. Twelve of 28 sites scattered in all seven areas have consistent axes of the maximum stiffness, and 12 other sites have dominant axes. Cortical bones with high

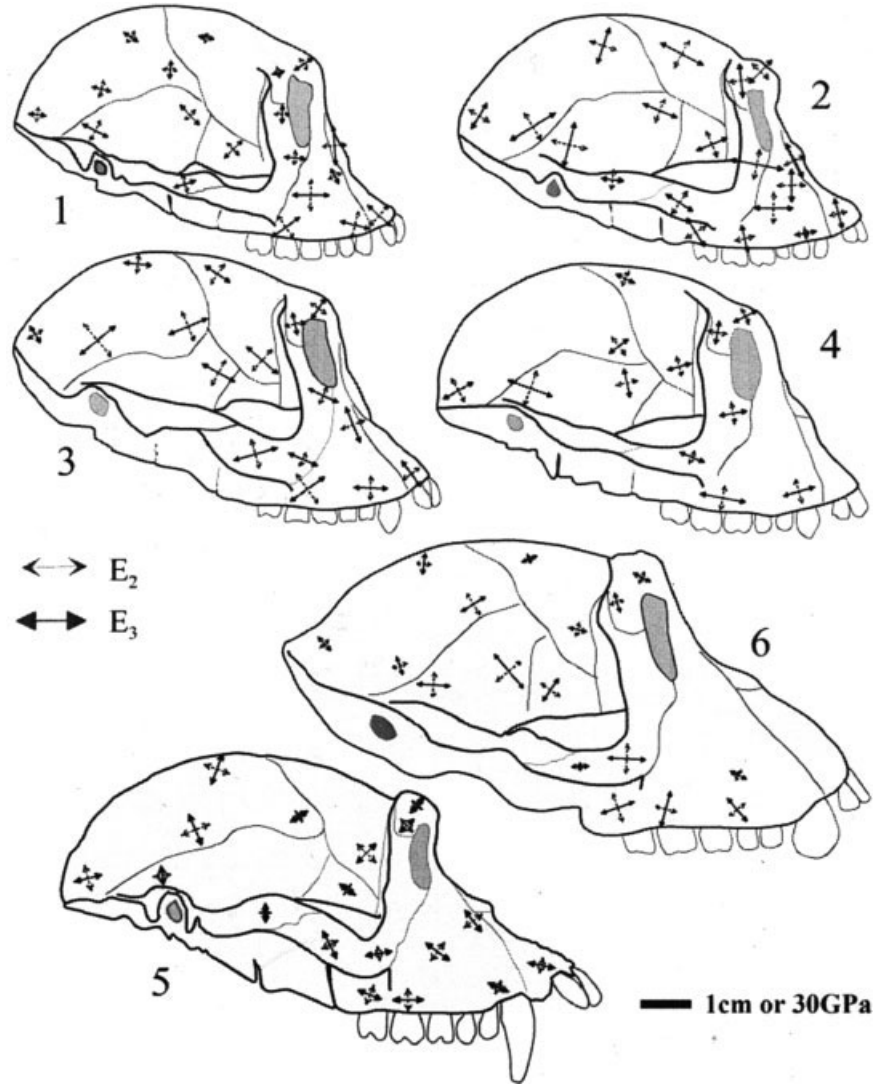


Fig. 3. Magnitude and orientation of maximum (E_3) and minimum (E_2) elastic moduli on cortical plane in six monkey crania.

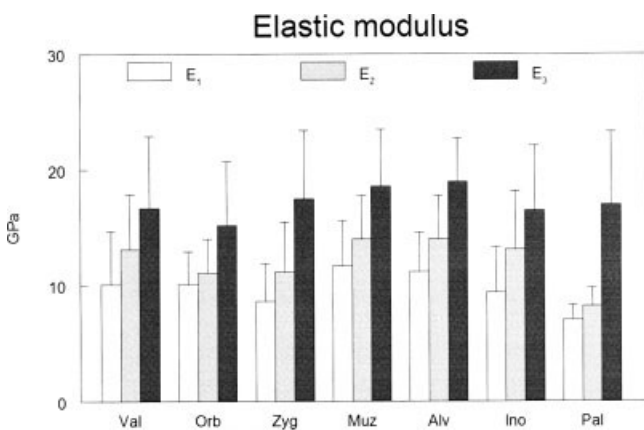


Fig. 4. Grand means of elastic moduli by areas. Error bar: SD.

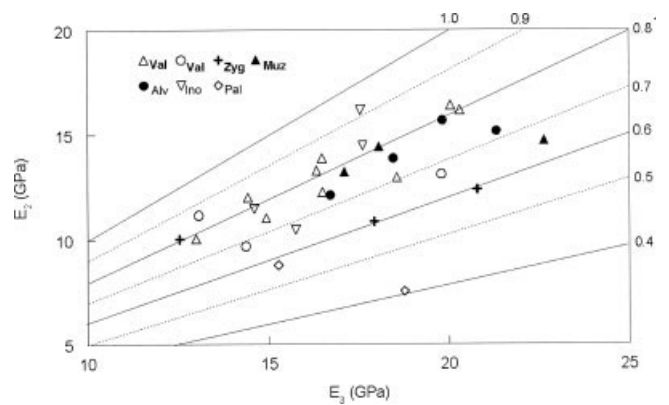


Fig. 5. Scatterplot of means of E_2 vs. E_3 . Correlation between E_2 and E_3 in a: $E_2 = 0.542 * E_3 + 3.275$, $r = 0.62$, $P < 0.001$.

E_2/E_3 anisotropy tend to have a consistent orientation of maximum stiffness across individuals. These regional features of bone elastic properties suggest functional differences.

Vault. The vault area includes the calvarial portion of the frontal bone, parietal bone, and greater wing of the sphenoid bone. The principal functions of this area are to protect the brain, and to provide a place of anchorage

TABLE 4. Anisotropy

Area	Site	E_1/E_2		E_1/E_3		E_2/E_3		
		Mean	SD	Mean	SD	Mean	SD	
Val	1	0.78	0.15	0.64	0.14	0.83	0.11	
	2	0.80	0.08	0.60	0.12	0.75	0.09	
	3	0.78	0.20	0.65	0.22	0.83	0.13	
	4	0.76	0.19	0.64	0.17	0.85	0.08	
	5	0.72	0.10	0.54	0.06	0.75	0.09	
	6	0.79	0.14	0.65	0.14	0.83	0.09	
	9	0.73	0.17	0.59	0.17	0.80	0.04	
	10	0.70	0.15	0.48	0.11	0.69	0.09	
	12	0.69	0.21	0.53	0.20	0.76	0.08	
	Total		0.75	0.15	0.59	0.15	0.79	0.10
	Orb	7	0.94	0.06	0.63	0.04	0.67	0.03
		8	0.92	0.04	0.79	0.08	0.87	0.08
15		0.86	0.05	0.60	0.12	0.70	0.14	
Total		0.91	0.06	0.68	0.11	0.75	0.12	
Zyg	11	0.82	0.14	0.65	0.18	0.79	0.19	
	13	0.68	0.13	0.40	0.08	0.58	0.06	
	14	0.83	0.07	0.49	0.08	0.59	0.13	
	Total		0.77	0.13	0.50	0.15	0.64	0.15
Muz	16	0.92	0.08	0.60	0.00	0.65	0.05	
	17	0.81	0.07	0.64	0.10	0.79	0.09	
	18	0.80	0.17	0.62	0.15	0.78	0.09	
	Total		0.83	0.12	0.62	0.10	0.76	0.09
Alv	19	0.80	0.19	0.63	0.13	0.79	0.06	
	20	0.83	0.13	0.59	0.10	0.71	0.12	
	21	0.81	0.13	0.58	0.16	0.71	0.14	
	22	0.75	0.16	0.54	0.05	0.74	0.16	
Total		0.80	0.14	0.58	0.11	0.73	0.12	
Ino	23	0.63	0.14	0.52	0.11	0.83	0.06	
	24	0.82	0.15	0.56	0.14	0.68	0.10	
	25	0.60	0.08	0.49	0.09	0.82	0.10	
	26	0.73	0.09	0.65	0.04	0.90	0.11	
Total		0.72	0.14	0.57	0.11	0.80	0.13	
Pal	27	0.86	0.11	0.51	0.14	0.59	0.09	
	28	0.86	0.06	0.40	0.17	0.45	0.17	
Total		0.86	0.09	0.45	0.16	0.52	0.15	
ANOVA		F	P	F	P	F	P	
Area		5.25	0.002	2.55	NS	4.41	0.005	
Site		1.71	0.028	2.16	0.003	4.74	0.001	

for the temporalis muscle. This part has relatively thick cortical bone, second only to the circumorbital area. The superior part (sites 1, 2, and 5) has a thicker external cortex than the inferior part (sites 4, 9, 10, and 12). However, their density is similar.

The average overall density in rhesus monkey skulls (1,699 mg/cm³) is significantly smaller than that in human dentate skulls (over 1,800 mg/cm³) (Peterson, 2002; Peterson and Dechow, 2003), indicating that macaque skull bones have less mineral content. How this is related to bone remodeling and adaptation to different physiological conditions is not clear. Many individuals in the human sample were aged adults, while the macaques were adult individuals with full occlusion. It is possible that relative age differences account for some of this difference in bone density.

The mean E_2/E_3 anisotropy in this area is weak. In trabecular bone, areas that are predominantly loaded in one direction are highly anisotropic, whereas areas that are loaded in varying directions are less anisotropic (Miller et al., 2002). However, this relationship is yet to be demonstrated in cortical bone.

Sites at the posterior and inferior portions of the vault have axes oriented parallel to a line between the superoposterior and inferoanterior regions of the vault, roughly

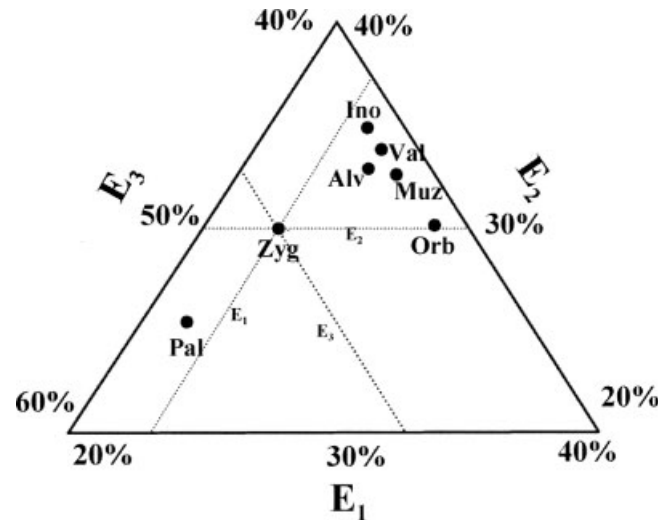


Fig. 6. Triangle plot of percentage of elastic moduli in three directions. Percentile value of modulus of each orthogonal direction is read at intersections of three lines passing through point of interest. Sums of E_1 , E_2 , and E_3 in each area are scaled to 100%. For example, in zygomatic arch, three principal mean elastic moduli are 8.6 GPa (E_1), 11.2 GPa (E_2), and 17.5 GPa (E_3); thus, relative values of E_1 , E_2 , and E_3 are 23%, 30%, and 47%, respectively.

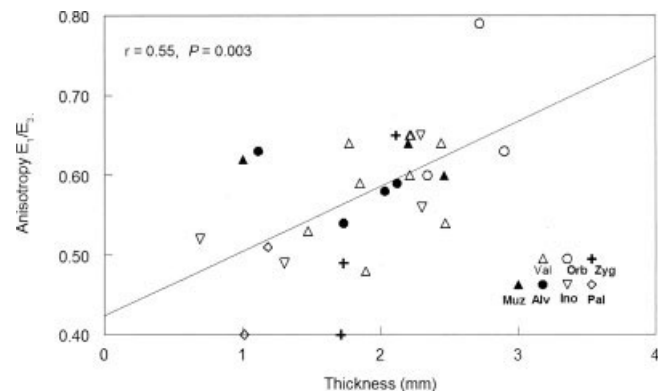


Fig. 7. Mean thickness vs. anisotropy (E_1/E_3) by site. Anisotropy (E_1/E_3) = 0.081 * Thickness + 0.424, $r = 0.50$, $P = 0.006$.

in the same direction as the presumed orientation of temporalis muscle force. The anterior part of the vault has an orientation roughly running anteroposteriorly.

Circumorbital area. The circumorbital area includes structures encircling the upper and lateral part of the orbital openings. The former is the supraorbital torus of the frontal bone, and the latter is composed of the zygomatic process of the frontal bone and the frontal process of the zygomatic bone. The principal functions of this area were suggested to be protection of the eyes and transmission of forces produced by mastication (Rak, 1983), though this was challenged by Ravosa et al. (2000), based on relatively weak in vivo strain measurements. This area has the thickest but least dense cortical bone of any cranial region. It also exhibits the least orthotropy, in that the difference in stiffness among three orthogonal axes is the smallest of any area.

TABLE 5. Direction of maximum stiffness (E_3)

Area	Site	Sites with consistent axis of E_3				Sites with dominant axis of E_3				
		N	Mean	SD	Uniformity P-value	N	Mean	SD	Uniformity P-value	
Val	1	6				3	76.3°	2.4°	0.033	
	2	6	110.4°	24.2°	0.046					
	3	6								
	4	5	153.1°	16.7°	0.019					
	5	6	5.0°	16.7°	0.007					
	6	6				3	21.7°	5.7°	0.040	
	9	6				3	51.6°	3.4°	0.036	
	10	6				4	61.2°	13.7°	0.030	
	12	6				3	137.2°	5.7°	0.040	
	Orb	7	6	102.0°	23.8°	0.042				
		8	6				4	75.9°	8.7°	0.014
	Zyg	15	6	20.6°	23.2°	0.037				
11		5	167.2°	17.7°	0.023					
Muz	13	6				3	19.0°	8.3°	0.049	
	14	6				4	47.3°	8.0°	0.013	
	16	6				5	13.7°	10.3°	0.005	
Alv	17	6	13.7°	6.6°	0.001					
	18	6	13.0°	16.3°	0.007					
	19	6								
Ino	20	6				4	103.6°	2.2°	0.049	
	21	6	24.0°	16.2°	0.006					
	22	6	10.6°	15.1°	0.005					
	23	4								
Pal	24	6	92.5°	20.8°	0.021					
	25	5				3	75.4°	8.8°	0.051	
	26	6				4	71.1°	6.5°	0.011	
Pal	27	6								
	28	6	89.8°	8.3°	0.001					

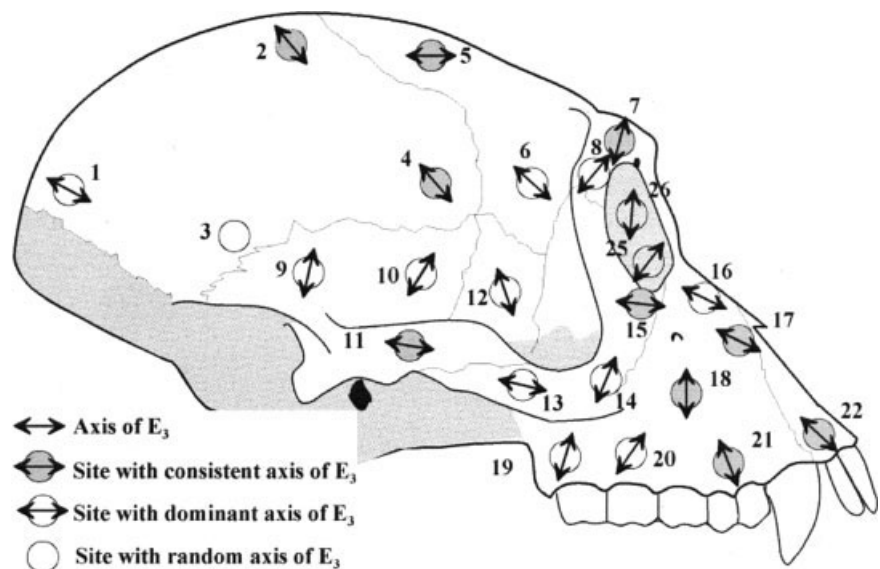


Fig. 8. Orientation of axes of maximum stiffness.

The axis of maximum stiffness is oriented similar to anatomical features on the superior and lateral borders of the orbit, running roughly tangential to the circumference of the orbit. In the supraorbital area, the dominant axis of maximum stiffness is oriented in the mediolateral direction. Bromage (1992) attempted to relate the distribution of preferentially oriented collagen in the macaque circumorbital region to in vivo and in vitro bone-strain data. He found that the preferential collagen fiber orientation was in general agreement with published observations in vivo and ex vivo masticatory-related surface strain for the supraorbital, lateral orbital, and infraorbital regions. As Bromage (1992) pointed out, this direc-

tion corresponds to the in vivo strain data of Hylander et al. (1991), which illustrated tension in the mediolateral direction. The lateral orbital region would resist tension inferosuperiorly or compression in the mediolateral direction. Both mean (20.6° to the sagittal plane) and dominant (25.2° to the sagittal plane) orientations are related to the lateral margin of the orbit. This agrees with observations on preferred osteon orientations in this area (Bromage, 1992).

Site 15 has a larger, although not significant, average E_3 than sites 7 and 8, comparable to a strain gradient observed in this area during in vivo experiments (Hylander and Johnson, 1997), though otherwise, in vivo

TABLE 6. Shear moduli

Area	Site	G ₁₂ (GPa)		G ₃₁ (GPa)		G ₃₂ (GPa)		
		Mean	SD	Mean	SD	Mean	SD	
Val	1	3.9	1.6	4.8	1.6	6.7	2.4	
	2	3.9	1.4	5.3	2.1	7.2	2.9	
	3	5.6	3.0	7.3	4.2	9.1	3.4	
	4	4.5	1.4	5.3	2.0	8.5	3.8	
	5	3.4	1.5	4.3	2.3	7.1	3.5	
	6	4.2	1.6	5.4	2.1	7.2	2.3	
	9	5.0	1.7	5.6	2.0	8.5	4.6	
	10	3.8	1.8	5.2	2.4	7.9	3.5	
	12	3.5	1.6	4.1	1.8	7.1	2.0	
	Total		4.2	1.8	5.2	2.3	7.7	3.0
	Orb	7	3.3	0.9	4.8	1.4	5.1	1.2
		8	4.3	1.4	5.1	1.9	6.0	1.8
15		4.4	1.5	6.4	2.2	8.0	2.5	
Total		3.9	1.3	5.3	1.8	6.2	2.1	
Zyg	11	3.1	1.1	3.8	1.1	4.9	1.6	
	13	4.2	1.9	4.6	1.5	8.6	2.8	
	14	3.7	1.7	5.3	1.2	8.6	3.3	
	Total		3.7	1.5	4.6	1.3	7.6	3.0
Muz	16	5.5	0.1	8.3	1.2	10.9	3.1	
	17	4.5	1.6	5.5	2.4	6.8	2.7	
	18	4.7	2.5	5.3	2.1	7.3	3.1	
	Total		4.8	1.7	6.0	2.3	7.8	3.0
Alv	19	4.8	1.6	6.7	3.0	7.9	2.0	
	20	5.0	1.3	6.1	1.7	7.9	3.2	
	21	4.3	1.7	5.8	2.4	7.4	2.1	
	22	4.4	1.1	5.2	1.0	7.3	1.9	
	Total		4.6	1.4	5.9	1.9	7.6	2.3
	Ino	23	4.1	1.7	4.3	1.7	6.4	1.3
24		3.4	0.8	4.4	1.4	6.3	1.8	
25		3.6	2.0	4.2	2.4	9.0	5.9	
26		5.0	2.4	5.4	2.3	7.4	3.3	
Total			4.0	1.7	4.6	1.8	7.1	3.0
Pal	27	2.6	0.4	2.8	0.4	3.6	0.9	
	28	2.2	0.4	2.5	0.4	3.3	0.9	
Total		2.4	0.4	2.6	0.5	3.4	0.9	
ANOVA		F	P	F	P	F	P	
Area		0.38	0.008	4.30	0.001	4.68	0.001	
Site		1.25	NS	1.57	NS	1.60	0.048	

TABLE 7. Poisson's ratios

Area	Site	v ₁₂		v ₁₃		v ₂₃		
		Mean	SD	Mean	SD	Mean	SD	
Val	1	0.39	0.13	0.27	0.15	0.23	0.14	
	2	0.46	0.08	0.29	0.11	0.16	0.09	
	3	0.35	0.18	0.22	0.19	0.16	0.14	
	4	0.44	0.07	0.35	0.11	0.22	0.18	
	5	0.49	0.12	0.27	0.14	0.18	0.18	
	6	0.41	0.10	0.32	0.19	0.15	0.11	
	9	0.30	0.08	0.23	0.12	0.22	0.14	
	10	0.43	0.04	0.20	0.12	0.23	0.07	
	12	0.46	0.10	0.36	0.09	0.20	0.30	
	Total		0.41	0.11	0.28	0.14	0.20	0.15
	Orb	7	0.46	0.08	0.14	0.10	0.21	0.09
		8	0.32	0.20	0.24	0.18	0.19	0.08
15		0.44	0.07	0.22	0.14	0.15	0.13	
Total		0.40	0.14	0.20	0.14	0.19	0.09	
Zyg	11	0.34	0.10	0.27	0.20	0.24	0.19	
	13	0.39	0.19	0.28	0.12	0.22	0.17	
	14	0.53	0.15	0.30	0.06	0.18	0.12	
	Total		0.43	0.16	0.29	0.12	0.21	0.14
Muz	16	0.35	0.09	0.13	0.15	0.11	0.04	
	17	0.28	0.18	0.28	0.11	0.16	0.08	
	18	0.37	0.13	0.24	0.09	0.15	0.13	
	Total		0.33	0.14	0.24	0.11	0.15	0.09
Alv	19	0.35	0.15	0.23	0.09	0.22	0.19	
	20	0.34	0.11	0.24	0.05	0.22	0.13	
	21	0.33	0.21	0.24	0.13	0.17	0.11	
	22	0.29	0.16	0.18	0.07	0.15	0.15	
	Total		0.33	0.15	0.22	0.09	0.19	0.13
	Ino	23	0.31	0.07	0.29	0.06	0.20	0.13
24		0.46	0.08	0.32	0.05	0.15	0.12	
25		0.46	0.12	0.40	0.11	0.23	0.16	
26		0.34	0.13	0.28	0.13	0.17	0.15	
Total			0.39	0.11	0.31	0.09	0.18	0.13
Pal	27	0.41	0.06	0.36	0.11	0.26	0.11	
	28	0.48	0.08	0.26	0.17	0.23	0.13	
Total		0.45	0.07	0.31	0.15	0.24	0.12	
ANOVA		F	P	F	P	F	P	
Area		1.85	NS	2.00	NS	0.54	NS	
Site		1.37	NS	1.02	NS	0.29	NS	

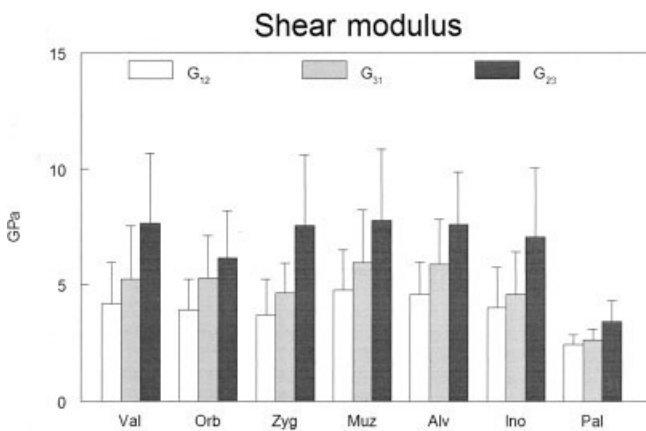


Fig. 9. Grand means of shear moduli by areas. Error bar: SD.

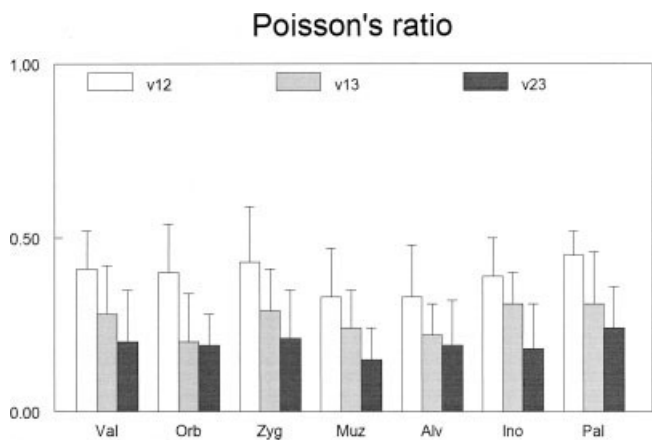


Fig. 10. Grand means of Poisson's ratios by areas. Error bar: SD.

strains were generally weak compared to other regions (Ravosa et al., 2000). However, average cortical thickness increases 24% from site 15 to site 7. Thus there is a thickness gradient, which is roughly opposite the direction of the strain gradient. Thickening of the cortex is an

effective way to decrease bone stress (Demes et al., 2000), although here the difference would only serve to increase the strain gradient. The nature of "low strain" of this area is certainly induced by the relatively higher

mass of bone in the region. However, the reason for this “overbuilt” phenomenon (Ravosa et al., 2000) is not clear.

Zygomatic arch. The zygomatic arch connects the lateral part of face and the skull. Its principal function is providing attachment of the masseter muscles. This area has larger anisotropies than all other regions of the skull, except for the palate.

Cortical stiffness and thickness increase anteroposteriorly, crossing the zygomaticotemporal suture. In vivo mechanical testing of the rhesus skull demonstrated the strain gradient in this area. Along the zygomatic arch, bone strains decrease anteroposteriorly (Hylander and Johnson, 1997). How these phenomena suggest bone adaptation to the local loading environment needs more study.

Muzzle area. The muzzle area is the superior lateral part of the snout, including the nasal bone, and the upper parts of the premaxillary and maxillary bones. This part protects the nasal cavity, and resists upward loads induced by biting forces (Rak, 1983). The cortex, as in other facial areas, is thinner than in the cranial vault. The axis of maximum stiffness, comparable to the situation in human maxillae (Peterson and Dechow, 2003), is oriented roughly parallel to the sagittal plane, which serves the function of resisting upwardly directed loads during biting or mastication.

Inner orbital area. The inner orbital area includes the four internal walls of the orbit, jointly formed in large part by the frontal, zygomatic, maxillary, and sphenoid bones. This area has the largest within-area variation in thickness and density. However, the difference in stiffness of the three orthogonal directions is small. All sites have an axis of maximum stiffness oriented perpendicular to the anteroposterior plane, with the exception of site 23, which has no statistically significant orientation among individuals.

The mechanism of the transmission of loads from the alveolar region to circumorbital bone has not received adequate study. In vivo investigations show low strain in the medial orbital wall and other thin bony parts around the orbit, which suggests that these structures are not optimally designed for resisting feeding forces (Ross, 2001). It was hypothesized that the function of this area is to provide rigid support and protection for soft tissues (Ross, 2001). Modeling of force transfer in these regions and the lateral orbit should help solve this problem. Little consideration here has been given to the effects of facial sutures in dampening masticatory loads and force transmission from the midface to the upper face.

Alveolar area. The alveolar area is the inferior lateral part of the facial skeleton, formed by maxillary and premaxillary bones. This area is the hosting organ for the maxillary teeth. This area has thin craniofacial bone, and differences in the stiffness of cortical bone in the three orthogonal directions are small. Both bone stiffness in three directions and its patterns of variation are comparable to those of the muzzle area, which might relate to the developmental and functional similarities of these regions. All axes of maximum stiffness run approximately superoinferiorly, as in human skulls (Peterson and Dechow, 2003). This orientation is the same as in the muzzle, and provides reduced deformation during masticatory or biting activities. These axes converge at

the level of the zygomatic bone or the lateral circumorbital pillar.

Palatal area. The palatine process of the maxilla forms most of the upper roof of the oral cavity, and stabilizes it during mastication. This area is unique in having the thinnest and densest cortical bone of any area, and having relatively small E_1 and E_2 compared to E_3 .

Exploration of the link between the form and function of the skull requires an understanding of 1) intrinsic forces acting on the skull, such as those forces generated during biting and mastication, and 2) extrinsic forces needed for head movement and maintenance of posture. However, knowledge of the direction and magnitude of those forces is insufficient for this purpose. The analysis of in vivo strain throughout the face of macaques indicates the clear absence of high strains and a uniform strain environment (Hylander and Johnson, 1997). This suggests that normal mechanical loads associated with chewing or biting likely have little effect on remodeling patterns in this region (Hylander and Johnson, 1997). However, this does not imply that these low strains are not needed to maintain bone structure and mass (Wood and Lieberman, 2001); nor does it imply that mechanical forces have not had evolutionary influences on craniofacial form (Daegling, 2004).

A difficulty with this study compared to previous investigations of human crania (Peterson, 2002; Schwartz-Dabney and Dechow, 2003) was a problem with obtaining adequate sample sizes of adult animals for study. Previous studies used samples ranging from 10–15 individuals. Here, a sample of six animals was obtained. This sample showed significant differences in many aspects of material properties. However, some of the more variable properties, such as E_3 , did not have differences that rose to the level of statistical significance. As the variation is similar to that in humans and the differences between sites and regions are similar to those in humans, it is likely that some of these differences will be shown to be significant if larger samples can be obtained. However, this study does show the large variability in elastic moduli between individuals at different sites.

Relationship between orientation of maximum stiffness and long axis of the bone

It is intriguing that cortical bones at sites with high anisotropy tend to have a constant axis of maximum stiffness in rhesus monkey skulls. Numerous investigators adopted the view that cortical bone is mechanically analogous to fiber-reinforced ceramic matrix composites. Osteons can be thought of as fibers within the larger bony matrix, with cement lines forming the interface between these constituents (Piekariski, 1970; Behiri and Bonfield, 1989), and anisotropy occurs due to nonrandom patterns of fiber orientation (Jacobs, 1994). The morphology of osteons is believed to be influenced by strain environment (Skedros et al., 1994). In human mandibles, apatite crystals are primarily oriented along the long axis of the corpus (Bacon et al., 1980). Likewise, in macaque mandibles and human femora, Haversian canals and most collagen fibrils are oriented parallel to the long axis (Bromage, 1993; Bromage and Boyde, 1998; Bromage et al., 2003; Goldman et al., 2003). These findings lead to the presumption that the orientation of maximum stiffness of cortical bone runs parallel to the anatomical axis of the bone. However, in macaque mandibles, the axis of

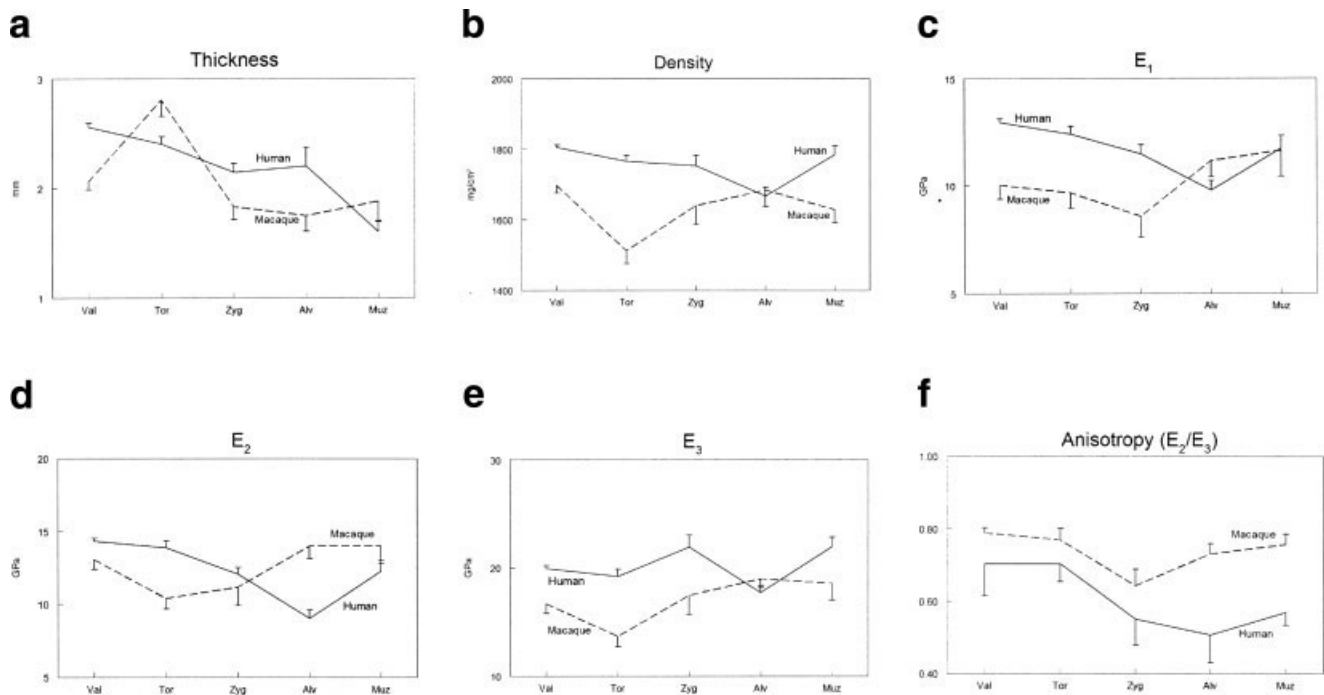


Fig. 11. Comparisons of cortical thickness (a), density (b) and elastic moduli E_1 (c), E_2 (d), E_3 (e) and Anisotropy (f) between rhesus monkey and human craniofacial skeleton. Error bar: SE. Abbreviations: Val-Vault; Tor-supraorbital torus; Zyg-Zygomatic arch; Alv-Alveolar area; Muz-Muzzle.

maximum stiffness is always at some angle to the long axis of the bone, which may decrease deformation during torsion (Dechow and Hylander, 2000). This was confirmed by studies in human skulls and baboon mandibles (Peterson, 2002; Peterson and Dechow, 2002, 2003; Schwartz-Dabney and Dechow, 2003; Wang and Dechow, 2004). This phenomenon echoes an assumption made by Jacobs (1994) that “it is not clear, however, how bone placement will not respond to the direction of mechanical force, nor whether bone mass will be proportional to the amount of strain provided by the bone.” Research documenting the response of the radius following removal of the ulna in sheep suggests that the greatest amount of bone deposition may not occur in areas of maximal strain, and may even continue when strain levels drop below normal (Lanyon et al., 1982), leading to the conjecture that the critical factor may be the distribution of strain (Lanyon et al., 1982; Rubin and Lanyon, 1982) or the rate of change of strain (O’Conner et al., 1982). Average directions of maximum stress and strain in complex bones, like those of facial skeletons, do not necessarily correspond with anatomical orientations or growth patterns (Jacobs, 1994) or with each other (Dechow and Hylander, 2000).

Comparison of cortical thickness, density, and material properties between human and rhesus monkey skulls

Previous studies inferred similarities in the elastic properties of mandibular cortical bone between more distantly related taxa, such as humans, baboons, and pigs (Dechow and Hylander, 2000; Wang and Dechow, 2004). As far as human and baboon mandibles are concerned, this is true in some regions, such as the ramus and the

lower border of the corpus, but not the mandible as a whole (Wang and Dechow, 2004).

Comparisons among cortical thickness, density, and material properties in rhesus monkey skulls and human skulls (data from Peterson, 2002; Peterson and Dechow, 2003) show that, overall, there are significant differences in cortical material properties between rhesus monkeys and human craniofacial skeletons (Fig. 11).

1. Vault and zygomatic arch: cortical bone in rhesus monkeys is thinner (this is obvious, considering the considerable size difference between human and macaques), less dense, and less stiff (except E_2) than in the human vault.
2. Supraorbital area: a similar pattern as in the vault is present, except that the cortical bone is relatively thicker in rhesus monkey skulls.
3. Alveolar area: the cortical bone is less thick, but denser and stiffer in rhesus monkey skulls than in human skulls.
4. Muzzle area: cortical bone is thicker, less dense and less stiff in the direction of maximum stiffness in rhesus monkey skulls.
5. Without exception, cortical bone in rhesus monkey skulls is more orthotropic than in human skulls in all comparable areas.

The axis of maximum stiffness for most bone regions is similar between species. For example, it runs medio-lateral in some sites in the vault, and suprainferiorly in the lower facial skeleton, and follows the anatomical long axis of the supraorbital torus and zygomatic arch.

These findings suggest that specific structural differences in skeletal form relate to differences in area-specific cortical material properties among species, but similarity

in general architecture of the cranium relates to a similar arrangement in the orientation of maximum stiffness.

Significance of intra- and interspecies variations for craniofacial mechanical modeling

The knowledge of exact material properties and their variation throughout the skull should improve the accuracy and precision of finite-element analysis (Strait et al., 2005). However, this study also demonstrated large variation among individuals. For example, the grand mean of the coefficient of variation of E_1 , E_2 , and E_3 among individuals is 36.7%, 31.6%, and 30.6%, respectively. This might suggest that in order to accurately simulate bone behaviors in a specific individual skull, the material properties must be assigned on an individual basis, together with other factors affecting biomechanics, such as cranial geometry, bone mass, and the modeling of patent sutures (Wang et al., 2005, 2006). However, these material properties data can be used to build up a model as a baseline for examining skull biomechanics in general, and studying regional functional morphology in particular.

The comparisons between baboon and human mandibles (Wang and Dechow, 2004), and between rhesus monkey and human crania, demonstrate a species-specific pattern of craniofacial material properties, which is more important than intraspecies variations when interspecies functional comparisons are done. We hypothesize that closely related species will have more similarities in patterns of bone material properties. This presumption would improve our confidence in simulating bone behaviors of primate fossil forms. Further work on related species, such as baboons and chimpanzees, is necessary here.

CONCLUSIONS

1. Thickness, density, and material properties of external cortical bone in rhesus monkey craniofacial skeletons were evaluated. Variations in features have functional implications.
2. Variation in the axes of maximum stiffness might mirror the complicated stress and strain environment of the cranium. There were significant orientations between individuals in some areas. The external cortical bones of the rhesus monkey skull can be modeled as orthotropic in some areas, and as transversely isotropic in the supraorbital region.
3. Cortical material properties differ between rhesus monkey and human craniofacial skeletons, which likely relates to differences in skeletal form and microstructure, and adaptation to different biomechanical environments.

ACKNOWLEDGMENTS

We sincerely thank the editors and two reviewers for providing valuable advice for improving the manuscript.

LITERATURE CITED

- Ashman RB. 1982. Ultrasonic determination of the elastic properties of cortical bone: techniques and limitations. Ph.D. dissertation, Tulane University.
- Ashman RB, Cowin SC, van Buskirk WC, Rice JC. 1984. A continuous wave technique for measurement of the elastic properties of cortical bone. *J Biomech* 17:349–361.
- Bacon GE, Bacon PJ, Griffiths RK. 1980. Orientation of apatite crystals in relation to muscle attachment in the mandible. *J Biomech* 13:725–729.
- Behrens RG, Carlson DS, Abdelnour T. 1978. In vivo analysis of bone strain about the sagittal suture in *Macaca mulatta* during masticatory movements. *J Dent Res* 57:904–908.
- Behiri JC, Bonfield W. 1989. Orientation dependence of the fracture mechanics of cortical bone. *J Biomech* 22:863–872.
- Bourne GH. 1975. The rhesus monkey. New York: Academic Press.
- Bromage TG. 1992. Microstructural organization and biomechanics of the macaque circumorbital region. In: Smith P, Tchernov E, editors. Structure, function and evolution of teeth. London: Freund Publishing House. p 257–272.
- Bromage TG, Boyde A. 1998. Intracortical remodeling and growth of the macaque mandible. *Scanning* 20:240.
- Bromage TG, Goldman HM, McFarlin SC, Warshaw J, Boyde A, Riggs CM. 2003. Circularly polarized light standards for investigations of collagen fiber orientation in bone. *Anat Rec* 274:157–168.
- Cooke MS, Wei SHY. 1991. Cephalometric errors: a comparison between repeat measurements and retaken radiographs. *Aust Dent J* 36:38–43.
- Daegling DJ. 2004. Relationship of strain magnitude to morphological variation in the primate skull. *Am J Phys Anthropol* 124:346–352.
- Dechow PC, Carlson DS. 1990. Occlusal force and craniofacial biomechanics during growth in rhesus monkeys. *Am J Phys Anthropol* 83:219–237.
- Dechow PC, Nail GA, Schwartz-Dabney CL, Ashman RB. 1993. Elastic properties of human supraorbital and mandibular bone. *Am J Phys Anthropol* 90:291–306.
- Dechow PC, Hylander WL. 2000. Elastic properties and masticatory bone stress in the macaque mandible. *Am J Phys Anthropol* 112:553–574.
- Demes B, Jungers WL, Walker C. 2000. Cortical bone distribution in the femoral neck of strepsirrhine primates. *J Hum Evol* 39:367–379.
- DeRousseau CJ. 1988. Osteoarthritis in rhesus monkeys and gibbons. Basel: Karger.
- Endo B. 1966. Experimental studies on the mechanical significance of the form of the human facial skeleton. *J Facult Sci Univ Tokyo* 3:1–101.
- Endo B. 1970. Analysis of stresses around the orbit due to masseter and temporalis muscles respectively. *Am J Anthropol Soc Nippon* 78:251–266.
- Evans F. 1973. Preservation effects. In: Evans F, editor. Mechanical properties of bone. Springfield, IL: Charles C. Thomas. p 56–60.
- Goldman HM, Bromage TG, Thomas CDL, Clement JG. 2003. Preferred collagen fibre orientation in the human mid-shaft femur. *Anat Rec* 272:434–445.
- Hylander WL, Johnson KR. 1997. In vivo bone strain patterns in the zygomatic arch of macaques and the significance of these patterns for functional interpretations of craniofacial form. *Am J Phys Anthropol* 102:203–232.
- Hylander WL, Picq PG, Johnson KR. 1991. Masticatory-stress hypothesis and the supraorbital region of primates. *Am J Phys Anthropol* 86:1–36.
- Jacobs CR. 1994. Numerical simulation of bone adaptation to mechanical loading. Ph.D. dissertation, Stanford University.
- Lanyon LE, Goodship AE, Pye CJ, MacFie JH. 1982. Mechanically adaptive bone remodeling. *J Biomech* 15:141–154.
- Miller Z, Fuchs MB, Arcan M. 2002. Trabecular bone adaptation with an orthotropic material model. *J Biomech* 35:247–256.
- Moss ML. 1976. The role of the nasal septal cartilage in midfacial growth. In: McNamara JA, editor. Factors affecting the growth of the midface. Ann Arbor: University of Michigan Press. p 169–204.
- O'Conner JA, Lanyon LE, MacFie H. 1982. The influence of strain rate on adaptive bone remodeling. *J Biomech* 15:767–781.
- Papadimitriou HM, Swartz SM, Kunz TH. 1996. Ontogenetic and anatomic variation in mineralization of the wing skeleton of the Mexican free-tailed bat, *Tadarida brasiliensis*. *J Zool Lond* 240:411–426.

- Peterson J. 2002. Cortical material properties of the human dentate and edentulous cranial complex. Ph.D. thesis, Baylor College of Dentistry, Texas A&M University System Health Science Center, Dallas, TX.
- Peterson J, Dechow PC. 2002. Material properties of the inner and outer cortical tables of the human parietal bone. *Anat Rec* 268:7–15.
- Peterson J, Dechow PC. 2003. Material properties of the human cranial vault and zygoma. *Anat Rec* 274:785–797.
- Piekarski K. 1970. Fracture of bone. *J Appl Physics* 41:215–223.
- Rak Y. 1983. The australopithecine face. New York: Academic Press.
- Ravosa MJ. 1991a. Ontogenetic perspective on mechanical and nonmechanical models of primate circumorbital morphology. *Am J Phys Anthropol* 85:95–112.
- Ravosa MJ. 1991b. Interspecific perspective on mechanical and nonmechanical models of primate circumorbital morphology. *Am J Phys Anthropol* 86:369–396.
- Ravosa MJ, Noble VE, Hylander WL, Johnson KR, Kowalski EM. 2000. Masticatory stress, orbital orientation and the evolution of the primate postorbital bar. *J Hum Evol* 38:667–693.
- Reilly DT, Burstein AH. 1975. The elastic and ultimate properties of compact bone tissue. *J Biomech* 8:393–405.
- Ross CF. 2001. In vivo function of the craniofacial haft: the interorbital “pillar.” *Am J Phys Anthropol* 116:108–139.
- Ross CF, Metzger KA. 2004. Bone strain gradients and optimization in vertebrate skulls. *Ann Anat* 186:387–396.
- Rubin CT, Lanyon LE. 1982. Limb mechanics as a function of speed and gait: a study of functional strains in the radius and tibia of horse and dog. *J Exp Biol* 101:187–211.
- Schneiderman ED. 1992. Facial growth in the rhesus monkey. Princeton: Princeton University Press.
- Schwartz-Dabney CL, Dechow PC. 2002a. Edentulation alters material properties of cortical bone in the human mandible. *J Dent Res* 81:613–617.
- Schwartz-Dabney CL, Dechow PC. 2002b. Accuracy of elastic property measurement in mandibular cortical bone is improved by using cylindrical specimens. *J Biomech Eng* 124:714–723.
- Schwartz-Dabney CL, Dechow PC. 2003. Variations in cortical material properties throughout the human dentate mandible. *Am J Phys Anthropol* 120:252–277.
- Shipman P, Walker A, Bichell D. 1985. The human skeleton. Cambridge, MA: Harvard University Press.
- Skedros J, Mason M, Bloebaum R. 1994. Differences in osteonal micromorphology between tensile and compressive cortices of a bending skeletal system: indications of potential strain-specific differences in bone microstructure. *Anat Rec* 239:405–413.
- Strait DS, Wang Q, Dechow PC, Ross CF, Richmond BG, Spencer MA, Patel BA. 2005. Modeling elastic properties in finite element analysis: how much precision is needed to produce an accurate model? *Anat Rec* 283:275–287.
- Sullivan WE. 1961. Skeleton and joints. In: Hartman CG, Straus WL Jr, editors. The anatomy of the rhesus monkey. New York: Nobel Offset Printers. p 43–84.
- Thayers TA. 1990. Effects of functional versus bisected occlusal planes on the “Wits” appraisal. *Am J Orthod Dentofacial Orthop* 9:422–426.
- Turner CH, Cowin SC. 1988. Errors induced by off-axis measurement of the elastic properties of bone. *J Biomech Eng* 110:213–215.
- van Buskirk WC, Cowin SC, Ward RN. 1981. Ultrasonic measurements of orthotropic elastic constants of bovine femoral bone. *J Biomech Eng Trans ASME* 103:67–71.
- Wang Q, Dechow PC. 2004. Variations in cortical material properties of baboon mandibles [abstract]. *Am J Phys Anthropol [Suppl]* 38:203.
- Wang Q, Dechow PC, Strait D, Ross C, Richmond B, Spencer M. 2005. In vitro strain of monkey facial sutures [abstract]. *Am J Phys Anthropol [Suppl]* 40:223.
- Wang Q, Dechow PC, Richmond B, Ross C, Spencer M, Strait D, Wright B. 2006. Fusion of craniofacial sutures in monkey skulls, with special reference to finite-element analysis [abstract]. *Am J Phys Anthropol [Suppl]* 42:184–185.
- Wood BA, Lieberman DE. 2001. Craniodental variation in *Paranthropus boisei*: a developmental and functional perspective. *Am J Phys Anthropol* 116:13–25.
- Yamada H, Evans FG. 1970. Strength of biological materials. Baltimore: Williams & Wilkins Co.
- Zar JH. 1999. Biostatistical analysis. 4th ed. Upper Saddle River, NJ: Prentice Hall.
- Ziopoulos P, Smith CW, An YH. 1999. Factors affecting mechanical properties of bone. In: An YH, Draughn RA, editors. Mechanical testing of bone and the bone-implant interface. Boca Raton, FL: CRC Press. p 87–101.